


Cite this: *RSC Adv.*, 2021, 11, 19666

# Creation of Mo/Tc@C<sub>60</sub> and Au@C<sub>60</sub> and molecular-dynamics simulations†

Tsutomu Ohtsuki,<sup>a</sup> Aaditya Manjanath,<sup>b</sup> Kaoru Ohno,<sup>c</sup> Makoto Inagaki,<sup>a</sup> Shun Sekimoto<sup>a</sup> and Yoshiyuki Kawazoe<sup>d</sup>

The formation of middle- and/or high-weight atom (Mo, Au)-incorporated fullerenes was investigated using radionuclides produced by nuclear reactions. From the trace radioactivities of <sup>99</sup>Mo/<sup>99m</sup>Tc or <sup>194</sup>Au after high-performance liquid chromatography, it was found that the formation of endohedral and/or heterofullerene fullerenes in <sup>99</sup>Mo/<sup>99m</sup>Tc and <sup>194</sup>Au atoms could occur by a recoil process following the nuclear reactions. Furthermore, the <sup>99m</sup>Tc (and <sup>194</sup>Au) atoms recoiled against β-decay remained present inside these cages. To confirm the produced materials experimentally, *ab initio* molecular dynamics (MD) simulations based on an all-electron mixed-basis approach were performed. The possibility of the formation of endohedral fullerenes containing Mo/Tc and Au atoms is verified; here, the formation of heterofullerenes is excluded by MD simulations. These findings suggest that radionuclides stably encapsulated by fullerenes could potentially play a valuable role in diagnostic nuclear medicine.

Received 3rd December 2020  
Accepted 19th May 2021

DOI: 10.1039/d0ra10196f

rsc.li/rsc-advances

## Introduction

Foreign-atom-encapsulating fullerenes are interesting materials because of their variety of functional uses. However, their utility depends strongly on the specific encapsulated elemental species. Therefore, the chemical affinity between C<sub>60</sub> and different elements is becoming an important field of research as new applications are identified.

To date, numerous experimental and theoretical studies of endohedrally (and references therein)<sup>1</sup> or exohedrally doped<sup>2–4</sup> fullerenes and heterofullerenes<sup>5–8</sup> with foreign atoms have been performed by utilizing arc-desorption or laser-vaporization techniques. However, it has also become possible to synthesize heterofullerenes in which foreign atoms are incorporated into the carbon cage.<sup>9,10</sup> Heterofullerenes doped with foreign atoms such as B,<sup>11,12</sup> N,<sup>13–15</sup> and Si<sup>16,17</sup> have been reported. In our previous studies, we investigated not only the endohedral doping of <sup>7</sup>Be,<sup>18</sup> <sup>79</sup>Kr, and <sup>127</sup>Xe,<sup>19</sup> but also the substitutional doping of <sup>11</sup>C,<sup>20</sup> <sup>13</sup>N,<sup>21</sup> <sup>69</sup>Ge, and <sup>72</sup>As<sup>22</sup> using a recoil-implantation process following nuclear reactions.

Despite extensive research, the formation process and the materials produced with respect to the nature of the chemical interaction between a foreign atom and a fullerene cage have been only partially clarified. This is because the synthesis of such new foreign-atom-encapsulating fullerene complexes is a complicated, multi-step process. Therefore, it is important to investigate their properties to advance the production of these complexes in several research fields. For example, Li@C<sub>60</sub> and N@C<sub>60</sub> are expected to be useful in molecular switch<sup>23</sup> and molecular qubit<sup>24</sup> applications, respectively.

In this paper, we present evidence of heavy Mo/Tc and Au atom-encapsulating fullerenes after collision between a C<sub>60</sub> cage and a Mo or Au atom. The collision was generated from recoil processes following nuclear reactions using the produced radionuclides, namely <sup>99</sup>Mo/<sup>99m</sup>Tc and <sup>194</sup>Au. We performed *ab initio* molecular dynamics (AIMD) simulations to determine whether the Mo/Tc and Au atoms can be encapsulated in fullerenes with endohedral doping: Mo@C<sub>60</sub>/Tc@C<sub>60</sub> and Au@C<sub>60</sub>, respectively. Studies on the chemical properties of these fullerenes encapsulating specific radioisotopes have been conducted,<sup>25–27</sup> and will be helpful in tailoring such promising materials for nuclear medical applications. We consider the most frequently used radionuclides in diagnostic nuclear medicine,<sup>28–30</sup> especially <sup>99m</sup>Tc, which is generally obtained by the decay of its parent radionuclide, <sup>99</sup>Mo. Another heavy element, Au (*e.g.*, <sup>198</sup>Au or <sup>194</sup>Au), can be regarded as a new candidate in related fields.<sup>31</sup>

## Experimental procedure

High-energy bremsstrahlung or charged-particle irradiation was used according to the source nuclide used.

<sup>a</sup>Institute for Integrated Radiation and Nuclear Science, Kyoto University, Asashiro-Nishi, Kumatori-cho, Sennan-gun, Osaka 590-0494, Japan. E-mail: ohtsuki.tsutomu.5c@kyoto-u.ac.jp

<sup>b</sup>Institute of Chemistry, Academia Sinica, 128 Academia Road, Section 2, Nankang, Taipei 11529, Taiwan. E-mail: aadityam@gate.sinica.edu.tw

<sup>c</sup>Department of Physics, Yokohama National University, 79-5 Tokiwadai, Hodogaya-ku, Yokohama 240-8501, Japan. E-mail: ohno@ynu.ac.jp

<sup>d</sup>New Industry Creation Hatchery Center, Tohoku University, 6-6 Aramaki, Aoba, Sendai 980-8579, Japan

† Electronic supplementary information (ESI) available. See DOI: 10.1039/d0ra10196f



(1) To produce  $^{99}\text{Mo}/^{99\text{m}}\text{Tc}$ -doped fullerenes, approximately 10 mg of  $\text{C}_{60}$  fullerene powder was mixed homogeneously with  $\text{CS}_2$  and 10 mg of a 97%-enriched  $^{100}\text{Mo}$  metal powder; the mixture was used as the target material. The samples were irradiated with a bremsstrahlung (high-energy  $\gamma$ -rays) of  $E_{\text{max}} = 30$  MeV, which originated from the bombardment of a Pt plate of 2 mm in thickness with an electron beam at an electron linear accelerator (LINAC), Laboratory of Nuclear Science, Tohoku University. The radioisotope of  $^{99}\text{Mo}$  can be produced by a photonuclear reaction, namely  $(\gamma, n)$ , by irradiating the enriched  $^{100}\text{Mo}$ . The irradiation time was set to approximately 8 h, and the average beam current was approximately 120  $\mu\text{A}$ . The sample was then cooled in a water bath during the irradiation. To confirm  $^{99}\text{Mo}$  production, the characteristic  $\gamma$ -rays from nuclear decay at 740 and 181 keV were measured using a Ge detector. The produced  $^{99}\text{Mo}$  decayed to  $^{99\text{m}}\text{Tc}$  with a 66 h half-life, and sequentially,  $^{99\text{m}}\text{Tc}$  decayed to  $^{99}\text{Tc}$ , emitting  $\gamma$ -rays at 140.5 keV. The decay process was confirmed using a Ge detector.

(2) To produce  $^{194}\text{Au}$ -doped fullerenes, approximately 10 mg of  $\text{C}_{60}$  fullerene powder was mixed homogeneously with 10 mg of a natural Pt metal powder (0.8–1.5  $\mu\text{m}$ ) and used as the target material. Deuteron irradiation with a beam energy of 16 MeV was performed at the Cyclotron Radio-Isotope Center, Tohoku University. The radioisotope  $^{194}\text{Au}$  can be produced by  $(d, 2n)$  reactions induced by irradiation. The deuteron beam current was typically 3  $\mu\text{A}$ , and the irradiation time was approximately 1 h. The target was cooled with circulated He gas during the irradiation. After irradiation, the samples were left for one day to allow the decay of short-lived radioactive byproducts. After one day of cooling, the radioactivity of  $^{194}\text{Au}$  could be measured with characteristic  $\gamma$ -rays at 328 keV, 294 keV, and so on.

The fullerene samples were dissolved in *o*-dichlorobenzene after filtration to remove insoluble materials through a membrane filter (pore size = 0.45  $\mu\text{m}$  and/or 0.2  $\mu\text{m}$ ). The soluble fraction was injected into a high-performance liquid chromatograph (HPLC) equipped with a 5PBB (silica-bonded with the pentabromobenzyl group) column of 10 mm (inner diameter)  $\times$  250 mm (length), at a flow rate of 2  $\text{mL min}^{-1}$  for the  $^{99}\text{Mo}/^{99\text{m}}\text{Tc}$  and 3  $\text{mL min}^{-1}$  for  $^{194}\text{Au}$  samples. The eluted solution was passed through an ultraviolet (UV) detector, the wavelength of which was adjusted to 290 nm to measure the quantity of fullerenes and their derivatives.

The fraction was collected at 30 s intervals, and the  $\gamma$ -ray activities of each fraction were measured with a Ge-detector coupled to a 4096-channel pulse-height analyzer with a conversion gain of 0.5 keV per channel. Therefore, the existence of  $^{99}\text{Mo}/^{99\text{m}}\text{Tc}$  and  $^{194}\text{Au}$  radioisotopes could be confirmed by their characteristic  $\gamma$ -rays.<sup>32</sup>

## Results and discussion

Fig. 1 shows three elution curves of the  $\text{C}_{60}$  sample irradiated by a bremsstrahlung of  $E_{\text{max}} = 30$  MeV. The horizontal axis indicates the retention time after injection into the HPLC system. The vertical axis indicates the  $\gamma$ -counting rate of the  $^{99}\text{Mo}/^{99\text{m}}\text{Tc}$  radioactivity, as measured with a Ge detector (counts per s), as

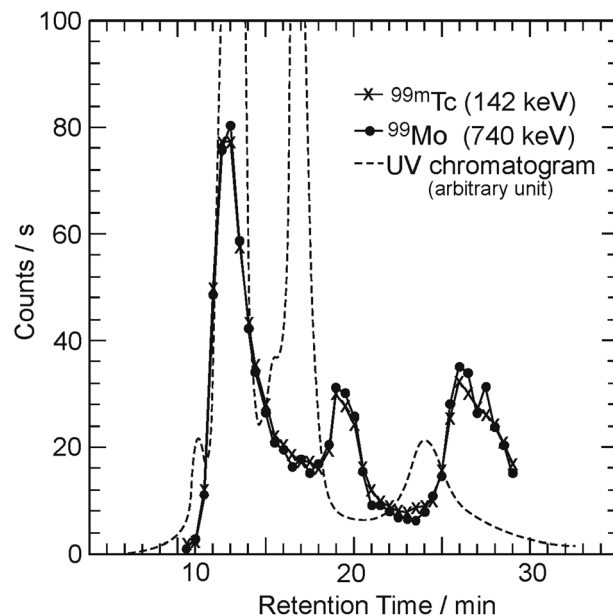


Fig. 1 HPLC elution curves of the soluble portion extracted in the  $\gamma$ -ray irradiated sample of  $\text{C}_{60}$  mixed with the enriched  $^{100}\text{Mo}$  metal powder. The horizontal axis indicates the retention time, and the vertical axis represents the counting rate of the radioactivities of  $^{99}\text{Mo}$  (solid circles)/ $^{99\text{m}}\text{Tc}$  (cross symbols) measured with a Ge detector and the absorbance of a UV chromatogram of  $\text{C}_{60}$  (dashed line).

well as the absorbances monitored continuously by a UV detector (dashed line, arbitrary unit). The solid circles and cross symbols represent the radioactivities of  $^{99}\text{Mo}$  and  $^{99\text{m}}\text{Tc}$ , respectively. A strong absorption peak was observed for a retention time of 12–14 min in the elution curve (dashed line: saturated), as measured using a UV detector. This peak position corresponds to the retention time of  $\text{C}_{60}$  (ultramarine blue in HPLC solution), which was confirmed in the calibration run using the  $\text{C}_{60}$  sample before irradiation. Following the first peak, two broad peaks at approximately 16–18 min (navy blue) and 22–26 min (brown) were observed in the UV chromatogram. The colors were reproduced well in each case.<sup>20,36</sup> Although there is a delay in the elution peaks of the radioactivities with respect to those of the UV absorption peaks, the elution behaviors appear similar. As  $^{99\text{m}}\text{Tc}$  is related to its radioactive equilibrium with  $^{99}\text{Mo}$ , the radioactive amount of  $^{99\text{m}}\text{Tc}$  is almost the same as that of  $^{99}\text{Mo}$ .

To characterize the components, the fraction corresponding to the second peak in Fig. 1 was collected and examined using matrix-assisted laser desorption/ionization time-of-flight (MALDI TOF) mass spectrometry. The mass spectrum of the fraction exhibited a series of peaks at  $m/z = 1440 - 24n$  ( $n = 1-4$ ) corresponding to the molecular ion peak of  $\text{C}_{120-n}\text{C}_2$ , in addition to the peak for  $\text{C}_{60}$  as a base peak.<sup>36</sup> This indicates that the second and smaller third peaks can be assigned to  $\text{C}_{60}$  dimers and  $\text{C}_{60}$  trimers, respectively. These materials can be produced by the interaction between  $\text{C}_{60}$  molecules in coalescence reactions after ionization by incident  $\gamma$ -rays or charged particles.<sup>20</sup>

The elution curves shown by the curve without symbols and by the curve with circles in Fig. 2 indicate the absorbance

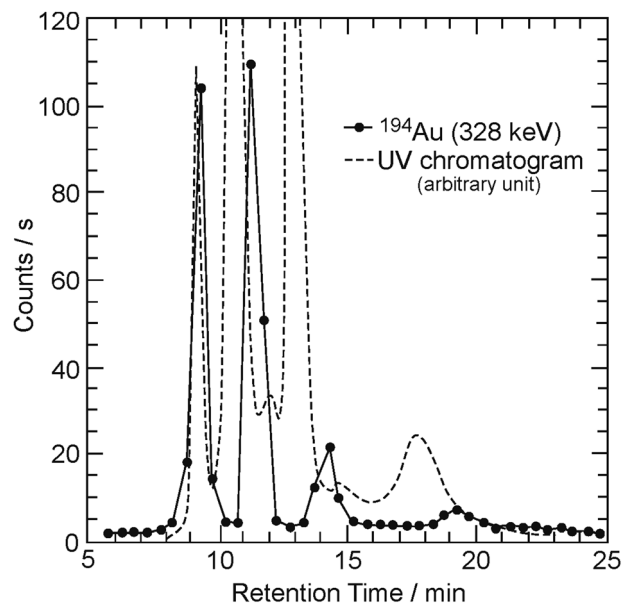


Fig. 2 Similar to Fig. 1, except that the counting rate is for radioactivities of  $^{194}\text{Au}$  (solid circle).

monitored continuously by a UV detector and the  $\gamma$ -counting rate of  $^{194}\text{Au}$  measured by a Ge-detector, respectively. The horizontal and vertical axes are the same as those shown in Fig. 1. Four populations of  $^{194}\text{Au}$  appear at retention times of 9 min, 10–11 min, approximately 13 min, and 17–19 min in Fig. 2. The ultramarine blue of  $\text{C}_{60}$  in the second fraction, the third fraction (navy blue), and the fourth fraction (brown) in the

UV chromatogram can be attributed to  $\text{C}_{60}$  monomers, dimers, and trimers, respectively, as indicated by the elution behavior of  $^{99}\text{Mo}/^{99\text{m}}\text{Tc}$ . The first peak (transparent) is due to the unknown byproducts of irradiation or UV spectrometry, despite the appearance of  $\gamma$  counts of  $^{194}\text{Au}$ . Therefore, this result indicates that radioactive fullerene monomers and their polymers (dimers and trimers) labeled with  $^{194}\text{Au}$  may exist in the final fractions. In our previous study, a similar trend was observed in the elution curves of the Kr, Xe, Ge, and As cases.<sup>19,22</sup> The quantity of the Mo/Tc-incorporated radioactive fullerenes produced here is estimated to be approximately  $10^{10}$ – $10^{12}$  molecules.

Here, it should be noted that no evidence of exohedral molecules was observed by extraction in the soluble portion. Exohedral molecules can be removed during solvation. Therefore, two possible molecular types should be considered in the present results: (1) endohedrally Mo/Tc atom-doped fullerenes,  $^{99}\text{Mo}@C_{60}/^{99\text{m}}\text{Tc}@C_{60}$  and  $^{194}\text{Au}@C_{60}$ ,<sup>18,19</sup> and (2) substitutional atom-doped heterofullerenes as a part of the cage,  $^{99}\text{MoC}_{59}/^{99\text{m}}\text{TcC}_{59}$  and  $^{194}\text{AuC}_{59}$ , as a result of As\*-C-59, As\*-C-69 (As\* = As-71, As-72, As-74), (GeC59)-Ge-69, and their polymers.<sup>22</sup>

To investigate the possibility of the formation of endohedral fullerenes and/or heterofullerenes in  $^{99}\text{Mo}/^{99\text{m}}\text{Tc}$  and  $^{194}\text{Au}$  atoms, we performed AIMD simulations to achieve greater clarity and distinction. The simulation configuration consisted of one  $\text{C}_{60}$  molecule and one Mo or Au atom. We assigned Mo (Au) with an initial  $E_{\text{kinetic}}$  of 40 eV (80 eV) at a distance of 5 Å from the  $\text{C}_{60}$  center along the  $z$ -direction impinging at the center of the topmost six-membered ring ( $x, y$ ) = (0, 0), where  $x$

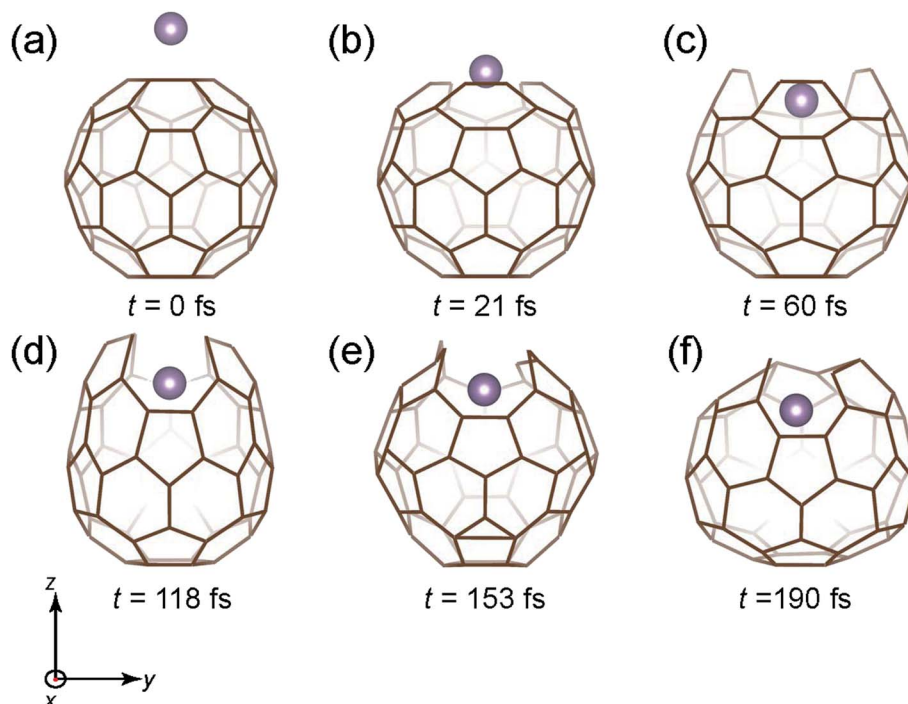


Fig. 3 Time snapshots of the  $\text{Mo} + \text{C}_{60} \rightarrow \text{Mo}@C_{60}$  simulation when the Mo atom vertically collides at the center of a six-member ring with an initial  $E_{\text{kinetic}}$  of 40 eV.



and  $y$  are the directions toward the center of a double bond and toward a carbon atom, respectively.

We employed the all-electron mixed-basis code TOMBO,<sup>19,33,34</sup> in which both plane waves (PWs) and numerical atomic orbitals (AOs) are used as basis functions. Local density approximation was used for the Mo + C<sub>60</sub> simulation, and the local spin-density approximation was used for the Au + C<sub>60</sub> simulation. The Perdew–Zunger form of the exchange–correlation potential<sup>35</sup> was used for both. A simple cubic unit cell with a 14 Å edge length was used. The cutoff energy for the PWs was 7 Ry, and the 1s, 2s, and 2p AOs were used for the C atoms, although the 2s and 2p AOs were confined inside the non-overlapping atomic sphere (NOAS) by subtracting a simple polynomial satisfying the matching condition at the surface of the NOAS. The subtracted smooth part that continues the original AO outside the NOAS can be simply expressed by a linear combination of PWs. The 1s, 2s, 2p, 3s, 3p, 3d, 5s, and 5p AOs were used for Mo, and the 1s, 2s, 2p, 3s, 3p, 3d, 4s, 4p, 4d, 4f, 5s, and 5p AOs were used for Au. This treatment ensures that two- or three-center integrals are not required between adjacent AOs and completely avoids the so-called basis-set superposition error. Moreover, the problem of over-completeness was significantly reduced using this procedure.<sup>35</sup>

Fig. 3 shows the time snapshots of the simulation, where the Mo atom attacks the C<sub>60</sub> molecule with a kinetic energy ( $E_{\text{kinetic}}$ ) of 40 eV. It hits the center of the six-membered ring at  $t = 21$  fs (Fig. 3(b)) and then slightly penetrates the C<sub>60</sub> cage at  $t = 60$  fs (Fig. 3(c)), where the six-membered ring expands to accommodate the incoming Mo atom while maintaining three C–C bonds. After a while ( $t = 118$ – $190$  fs), the cage structure is

gradually recovered (Fig. 3(d)–(f)), and the Mo atom is fully encapsulated.

However, if  $E_{\text{kinetic}}$  is increased to 80 eV, the Mo atom is not encapsulated, as shown in Fig. 4. The situation is similar to that of the 40 eV case (Fig. 3) up to 21 fs, where the cage structure opens up. Beyond 21 fs, owing to the high  $E_{\text{kinetic}}$  of the atom, the cage structure is gradually destroyed (Fig. 4(c)–(f)), eventually leading to no encapsulation of the atom.

In contrast, when we impose the same  $E_{\text{kinetic}}$  of 80 eV on the Au atom toward the center of the six-membered ring, the structure of the cage is preserved with Au encapsulation.

Fig. 5 shows the time snapshots of this simulation for Au + C<sub>60</sub> → Au@C<sub>60</sub>. It hits the center of the six-membered ring at  $t = 27$  fs (Fig. 5(b)), and then slightly goes inside at  $t = 60$  fs (Fig. 6(c)), when the six-membered ring expands while keeping three C–C bonds, similar to the case of Mo encapsulation at 40 eV (Fig. 5(c)). The cage structure is recovered at  $t = 130$ – $170$  fs (Fig. 5(d) and (e)), and the Au atom penetrates deep inside the cage at  $t = 249$  fs (Fig. 5(f)).

To verify whether the Mo/Au atom continued to remain encapsulated or destroyed the cage, we performed MD simulations for much longer durations. We found that the atoms moved around in the cage owing to their  $E_{\text{kinetic}}$  values, but remained encapsulated. Therefore, it is reasonable to expect that at timescales longer than the picosecond regime, there would be no change in the encapsulation scenario. This fact supports the identification of the experimentally observed incorporated fullerenes as endohedral fullerenes of <sup>99</sup>Mo/<sup>99m</sup>Tc and <sup>194</sup>Au atoms.

For a more comprehensive understanding, a schematic view of the reaction process in the target material is shown in Fig. 6.

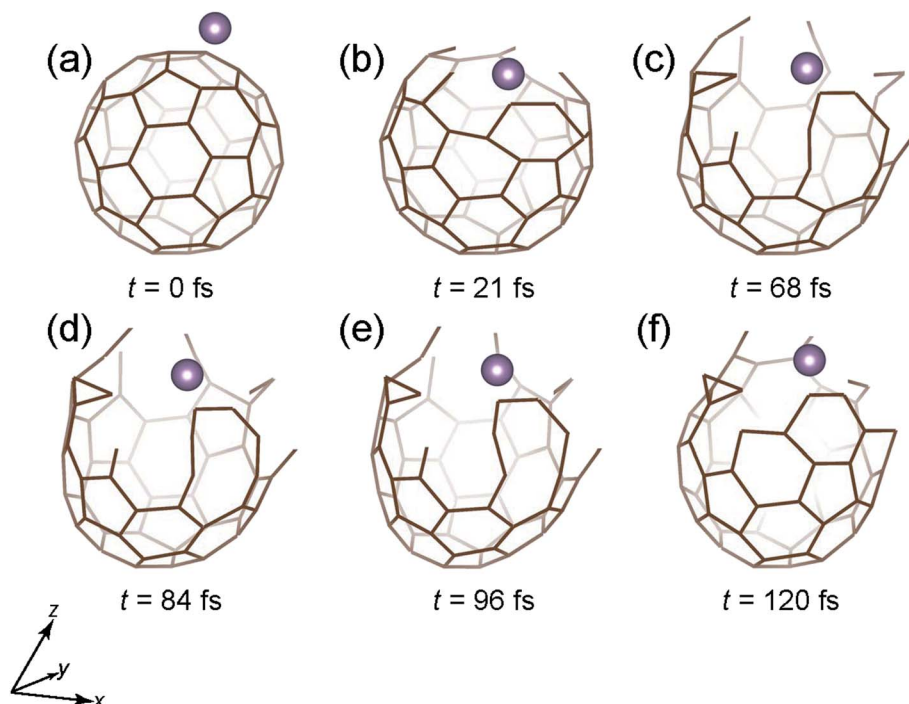


Fig. 4 Time snapshots of the Mo + C<sub>60</sub> → Mo + C<sub>60</sub> (broken) simulation when the Mo atom vertically collides at the center of a six-member ring with an initial  $E_{\text{kinetic}}$  of 80 eV.



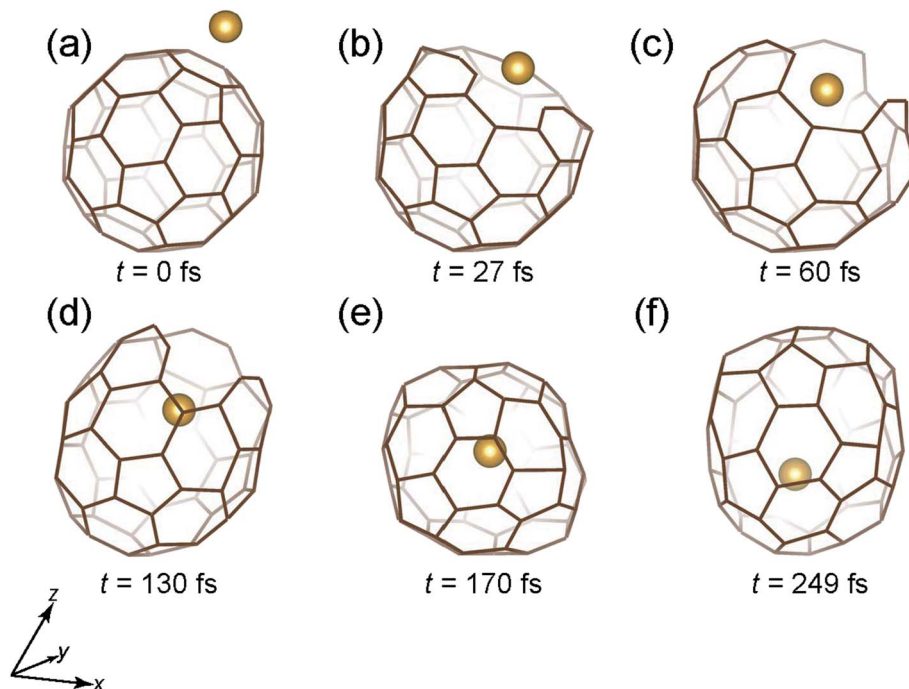


Fig. 5 Time snapshots of the  $\text{Au} + \text{C}_{60} \rightarrow \text{Au@C}_{60}$  simulation when an Au atom vertically collides at the center of a six-member ring with an initial  $E_{\text{kinetic}}$  of 80 eV.

The experimental results presented here support the following scenario (here, for example, in the case of  $^{100}\text{Mo}(\gamma, n)^{99}\text{Mo} \rightarrow \beta^- \rightarrow ^{99\text{m}}\text{Tc}$ ). Several radioactive nuclides are produced by  $(\gamma, n)$  (and  $(d, 2n)$  for  $^{194}\text{Au}$ ) reactions. The  $E_{\text{kinetic}}$  values of the radionuclides are of similar orders of magnitude, even in different nuclear reactions. The form of the emitted neutron spectrum is expected to be approximately Maxwellian in distribution and the average neutron  $E_{\text{kinetic}}$  seems to be approximately 2–3 MeV, while the initial  $E_{\text{kinetic}}$  of the recoiled

nuclides is estimated to be approximately a few hundred kilo-electron volts, even if the reaction is accompanied by two neutron emissions. The energetic nuclides should destroy the fullerene cages because  $E_{\text{kinetic}}$  is estimated to be of a different order of magnitude than the energies (some electron volts) of molecular bonding. Therefore, the atoms being produced escape from their own material owing to the  $E_{\text{kinetic}}$  of approximately a few hundred kilo-electron volts. Then,  $E_{\text{kinetic}}$  is reduced in the sample to a magnitude appropriate for

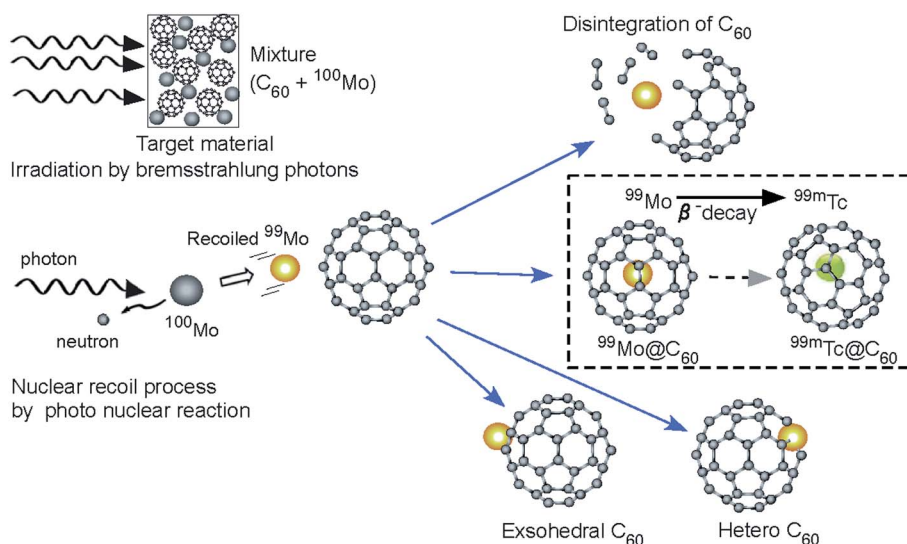


Fig. 6 Schematic image in the  $\text{Mo} + \text{C}_{60}$  for the recoil process by photonuclear reactions  $(\gamma, n)$  is shown using the  $^{100}\text{Mo}$  irradiated by bremsstrahlung photons (high-energy photons:  $\gamma$ ).



incorporation. Finally, the radionuclides hit the C<sub>60</sub> cages, as shown in Fig. 3, and stop in the cage, thus forming endohedral fullerenes or heterofullerenes. Furthermore, the shock produces fullerene polymers by inducing interactions with neighboring fullerene cages.<sup>18–22</sup>

After encapsulation, recoil destruction may occur inside the fullerene; specifically, the radioactive species <sup>99</sup>Mo/<sup>99m</sup>Tc and <sup>194</sup>Au can decay *via* β or γ emission to daughter nuclides *via* the reactions <sup>99</sup>Mo → β<sup>−</sup> → <sup>99m</sup>Tc (radioactive equilibrium) and <sup>99m</sup>Tc → γ → <sup>99</sup>Tc (140.5 keV; ground state), and <sup>194</sup>Au → β<sup>+</sup> → <sup>194</sup>Pt (stable nuclide). If we consider the nuclear recoil by β-decay and/or γ-ray from an energetic perspective, we must consider the following important issues: (1) the contribution of the nuclear recoil process to reducing energy inside the C<sub>60</sub> and (2) the reaction pathway for the radionuclide in exiting the C<sub>60</sub> and destroying the host cages. The maximum energy of the β-ray in <sup>99</sup>Mo was 1.214 MeV. Therefore, the maximum recoil energy of the radionuclides (*i.e.*, <sup>99m</sup>Tc with β-decay and subsequent γ-ray emissions from <sup>99</sup>Mo) is estimated to be much lower than a few tens of electron volts,<sup>37–40</sup> even in <sup>194</sup>Au → β<sup>+</sup> → <sup>194</sup>Pt and subsequent γ-ray emissions. Here, the recoil process occurs inversely from within the C<sub>60</sub> cage to exit, and the motion is similar to that during the insertion process from the outside. The radioactive equilibrium between <sup>99</sup>Mo and <sup>99m</sup>Tc was complete, and the radioactive amounts were approximately the same (see Fig. 1). This fact may indicate that the <sup>99m</sup>Tc atoms (and even those in <sup>194</sup>Pt) recoiled against β-decay (β<sup>+</sup>-decay), and subsequently, γ-rays remained inside these cages to create <sup>99m</sup>Tc (<sup>194</sup>Pt) endohedral C<sub>60</sub>. Here, electronegativity may play an important role in the incorporation of middle- and/or heavy-weight atoms. Finally, it is interesting to note that if <sup>99</sup>Mo/<sup>99m</sup>Tc and <sup>194</sup>Au can be successfully carried by a C<sub>60</sub> cage to a certain organ, it may be effectively used for diagnosis and treatment. Furthermore, radioisotopes used in nuclear medicine (not only <sup>99</sup>Mo/<sup>99m</sup>Tc or <sup>194</sup>Au, but also, <sup>47</sup>Sc, <sup>64,67</sup>Cu, <sup>68</sup>Ga, <sup>105</sup>Rh, <sup>177</sup>Lu, and <sup>188</sup>Re)<sup>29</sup> are intriguing for encapsulation applications. These findings further indicate that radionuclide-encapsulating fullerenes have high potential for applicability in radioimmunotherapy; in particular, the physical and/or chemical properties of the radionuclide-encapsulating fullerenes could be superior to those of conventional chelating chemicals for medical use.

## Conclusions

The formation of (Mo, Au)-encapsulating fullerenes was investigated using radionuclides produced by nuclear reactions. From the trace radioactivities of <sup>99</sup>Mo/<sup>99m</sup>Tc or <sup>194</sup>Au after HPLC, it was observed that endohedral fullerenes and/or heterofullerene in <sup>99</sup>Mo/<sup>99m</sup>Tc and <sup>194</sup>Au atoms can form through a recoil process following nuclear reactions. To verify the production of these materials, AIMD simulations based on an all-electron mixed-basis approach were performed. Our combined experimental and theoretical results strongly support the interpretation that endohedral fullerenes encapsulating Mo/Tc and Au atoms were formed. Furthermore, we found that the <sup>99m</sup>Tc (and even <sup>194</sup>Au) atoms recoiled against β-decay can

remain inside these cages. Fullerenes could potentially play a valuable role in diagnostic nuclear medicine by stably encapsulating radionuclides.

## Conflicts of interest

There are no conflicts to declare.

## Acknowledgements

This study was supported by the NEDO project (No. 16101402-0), Kakenhi (No. 16K15579, No. 18H04150, No. 19K22596, No. 18H01939 in Grants-in-Aid for Scientific Research), and KAN-GENKON. We are also indebted to the HPCI promoted by MEXT for the use of the supercomputer SR16000 at Hokkaido University and at IMR, Tohoku University (Project IDs. hp170268 and hp170190). We are grateful for the assistance of the technical staff of the Laboratory of Nuclear Science and the Cyclotron, Tohoku University, for beam handling.

## Notes and references

- 1 A. A. Popov, S. Yang and L. Dunsch, *Chem. Rev.*, 2013, **113**, 5989–6113.
- 2 L. M. Roth, Y. Huang, J. T. Schwedler, C. J. Cassidy, D. Ben-Amotz, B. Kahr and B. S. Freiser, *J. Am. Chem. Soc.*, 1991, **113**, 6298–6299.
- 3 Y. Huang and B. S. Freiser, *J. Am. Chem. Soc.*, 1991, **113**, 9418.
- 4 S. W. McElvany, *Journal of Physical Chemistry Chemical Physics*, 1992, **96**, 4935–4937.
- 5 S. Ostrowski, M. H. Jamrz and J. Cz. Dobrowolski, *Tetrahedron: Asymmetry*, 2013, **24**, 1097–1109.
- 6 R. Yu, M. Zhan, D. Cheng, S. Yang, Z. Liu and L. Zheng, *Journal of Physical Chemistry Chemical Physics*, 1995, **99**, 1818–1819.
- 7 Y. Hashikawa, M. Murata, A. Wakamiya and Y. Murata, *J. Am. Chem. Soc.*, 2016, **138**, 4096–4104.
- 8 O. Vostrowsky and A. Hirsch, *Chem. Rev.*, 2006, **106**, 51915207.
- 9 S. Jalife, J. Arcudia, S. Pan and G. Merino, *Chem. Sci.*, 2020, **11**, 6642–6652.
- 10 K. Ohno, A. Manjanath, Y. Kawazoe, R. Hatakeyama, F. Misaizu, E. Kwon, H. Fukumura, H. Ogasawara, Y. Yamada, C. Zhang, N. Sumi, T. Kamigaki, K. Kawachi, K. Yokoo, i S. Ono and Y. Kasama, *Nanoscale*, 2018, **10**, 1825–1836.
- 11 T. Guo, C. Jin and R. E. Smalley, *Journal of Physical Chemistry Chemical Physics*, 1991, **95**, 4948–4950.
- 12 H.-J. Muhr, R. Nesper, B. Schnyder and R. Kötz, *Chem. Phys. Lett.*, 1996, **249**, 399–405.
- 13 T. Pradeep, V. Vijayakrishnan, A. K. Santra and C. N. R. Rao, *Journal of Physical Chemistry Chemical Physics*, 1991, **95**, 10564–10565.
- 14 J. F. Christian, Z. Wan and S. L. Anderson, *Journal of Physical Chemistry Chemical Physics*, 1992, **96**, 10597–10600.
- 15 H. Huang, G. Zhang, D. Wang, N. Xin, S. Liang, N. Wang and L. Gan, *Angew. Chem.*, 2013, **52**, 5037–5040.



- 16 M. Pellarin, C. Ray, P. Mélinon, J. Lermé, J. L. Vialle, P. Kéghélian, A. Perez and M. Broyer, *Chem. Phys. Lett.*, 1997, **277**, 96–104.
- 17 C. Ray, M. Pellarin, J. L. Lermé, J. L. Vialle, M. Broyer, X. Blase, P. Mélinon, P. Kéghélian and A. Perez, *Phys. Rev. Lett.*, 1998, **80**, 5365–5368.
- 18 T. Ohtsuki, K. Masutomo, K. Ohno, Y. Maruyama, Y. Kawazoe, K. Sueki and K. Kikuchi, *Phys. Rev. Lett.*, 1996, **77**, 3522–3524.
- 19 T. Ohtsuki, K. Ohno, K. Shiga, Y. Kawazoe, Y. Maruyama and K. Masutomo, *Phys. Rev. Lett.*, 1998, **81**, 967–970.
- 20 T. Ohtsuki, K. Masutomo, K. Sueki, K. Kobayashi and K. Kikuchi, *J. Am. Chem. Soc.*, 1995, **117**, 12869–12870.
- 21 T. Ohtsuki, K. Masutomo, K. Sueki, K. Shikano and T. Shigematsu, *J. Radioanal. Nucl. Chem.*, 1999, **239**, 365–370.
- 22 T. Ohtsuki, K. Ohno, K. Shiga, Y. Kawazoe, Y. Maruyama and K. Masumoto, *Phys. Rev. B*, 1999, **60**, 1531–1534.
- 23 H. J. Chandler, M. Stefanou, E. E. B. Campbell and R. Schaub, *Nat. Commun.*, 2019, **10**, 2283.
- 24 S. R. Plant, M. Jevric, J. J. L. Morton, A. Ardavan, A. N. Khlobystov, G. A. D. Briggs and K. Porfyrakis, *Chem. Sci.*, 2013, **5**, 2971.
- 25 M. D. Diener, J. M. Alford, S. J. Kennel and S. Mirzadeh, *J. Am. Chem. Soc.*, 2007, **129**, 5131–5138.
- 26 Z. Chen, L. Ma, Y. Liu and C. Chen, *Theranostics*, 2012, **2**, 38–50.
- 27 R. D. Bolskar, *Encyclopedia of Nanotechnology, Fullerenes for Drug Delivery*, 2016, pp. 1267–1281.
- 28 M. Inagaki, S. Sekimoto, T. Tadokoro, Y. Ueno, Y. Kani and T. Ohtsuki, *J. Radioanal. Nucl. Chem.*, 2020, **324**, 681–686.
- 29 M. Inagaki, S. Sekimoto, W. Tanaka, T. Tadokoro, Y. Ueno, Y. Kani and T. Ohtsuki, *J. Radioanal. Nucl. Chem.*, 2019, **322**, 1703–1709.
- 30 J. Jang, H. Kikunaga, S. Sekimoto, M. Inagaki, T. Kawakami, T. Ohtsuki, S. Kashiwagi, K. Takahashi, K. Tsukada, K. Tatenuma and M. Uesaka, *Nucl. Instrum. Methods Phys. Res., Sect. A*, 2021, **987**, 164815.
- 31 D. Maccora, V. Dini, C. Battocchio, I. Fratoddi, A. Cartoni, D. Rotili, M. Castagnola, R. Faccini, I. Bruno, T. Scotognella, A. Giordano and I. Venditti, *Appl. Sci.*, 2019, **9**, 1–23.
- 32 S. Y. F. Chu, L. P. Ekström and R. B. Firestone, *Table of Isotopes, The Lund/LBNL Nuclear Data Search, Version 2.0*, 1999.
- 33 K. Ohno, F. Mauri and S. G. Louie, *Phys. Rev. B: Condens. Matter Mater. Phys.*, 1997, **56**, 1009–1012.
- 34 S. Ono, Y. Noguchi, R. Sahara, Y. Kawazoe and K. Ohno, *Comput. Phys. Commun.*, 2015, **189**, 20–30.
- 35 J. P. Perdew and A. Zunger, *Phys. Rev. B: Condens. Matter Mater. Phys.*, 1981, **23**, 5048–5079.
- 36 T. Ohtsuki, K. Masutomo, T. Tanaka and K. Komatsu, *Chem. Phys. Lett.*, 1999, **300**, 661–666.
- 37 K. Sueki, K. Akiyama, K. Kikuchi, H. Nakahara and K. Tomura, *Chem. Phys. Lett.*, 1998, **288**, 179–182.
- 38 G. E. Gadd, P. Schmidt, C. Bowles, G. McOrist, P. J. Evans, J. Wood, L. Smith, A. Dixon and J. Easey, *J. Am. Chem. Soc.*, 1998, **120**, 10322–10325.
- 39 T. Braun and H. Rausch, *Chem. Phys. Lett.*, 1998, **288**, 179–182.
- 40 T. A. Carlson, *Phys. Rev.*, 1963, **132**, 2239–2242.

